

# Page Proof Instructions and Queries

**Journal Title:** SIM  
**Article Number:** 1109570

Thank you for choosing to publish with us. This is your final opportunity to ensure your article will be accurate at publication. Please review your proof carefully and respond to the queries using the circled tools in the image below, which are available in Adobe Reader DC\* by clicking **Tools** from the top menu, then clicking **Comment**.

Please use *only* the tools circled in the image, as edits via other tools/methods can be lost during file conversion. For comments, questions, or formatting requests, please use . Please do *not* use comment bubbles/sticky notes .



\*If you do not see these tools, please ensure you have opened this file with **Adobe Reader DC**, available for free at [get.adobe.com/reader](http://get.adobe.com/reader) or by going to Help >Check for Updates within other versions of Reader. For more detailed instructions, please see [us.sagepub.com/ReaderXProofs](http://us.sagepub.com/ReaderXProofs).

Sl. No.	Query
	Please note that we cannot add/amend orcid ids for any article at the proof stage. following orcid's guidelines, the publisher can include only orcid ids that the authors have specifically validated for each manuscript prior to official acceptance for publication.
	Please confirm that all author information, including names, affiliations, sequence, and contact details, is correct.
	Please review the entire document for typographical errors, mathematical errors, and any other necessary corrections; check headings, tables, and figures.
	Please ensure that you have obtained and enclosed all necessary permissions for the reproduction of artworks (e.g. illustrations, photographs, charts, maps, other visual material, etc.) not owned by yourself. please refer to your publishing agreement for further information.
	Please note that this proof represents your final opportunity to review your article prior to publication, so please do send all of your changes now.
	Please confirm that the acknowledgement and funding statements are accurate.
1	'Koshi et al.' does not match with Ref. 21. Please check and correct.
2	Please provide description for the part labels mentioned in the artwork of Figure 3.
3	Please check the edits made to the caption of Figure 4.
4	Please check whether Tables 3 and 4 are correct as set.
5	Please check whether Table 6 is correct as set.

# Numerical exploration of freeway tunnel effects with a two-lane traffic model

Zhengming Li<sup>1,2</sup>, M N Smirnova<sup>3</sup>, Yongliang Zhang<sup>1</sup>,  
N N Smirnov<sup>3</sup> and Zuojin Zhu<sup>1,3</sup> 

## Abstract

To explore freeway tunnel effects on ring road traffic flow, a two-lane traffic model is put forward. The model adopts lane-changing time to describe the net lane-changing rate, assuming that the time is approximately equal to the relaxation time of traffic flow, but infinite when the absolute value of difference of traffic density between the two lanes is lower than 1 veh/km, as it is hard for car drivers to perceive such a small difference. Based on the two-lane traffic model, a simulation platform is built to predict traffic flow on a two-lane freeway ring with a tunnel of 0.3 km length having a speed limit of 80 km/h, and free flow speeds on lane I and II equal to 120 and 100 km/h, respectively. The platform uses a third-order Runge–Kutta scheme to handle the time derivative term, and a fifth-order weighted essentially non-oscillatory scheme to calculate numerical flux. Simulation results show that the freeway tunnel can trigger traffic shock originating at the entrance when the coming flow density is beyond a traffic density threshold that is dependent on the off-ramp flow just upstream the tunnel. The occurrence of traffic shock leads to the mean travel time through the tunnel is almost a constant when the initial density normalized by jam density is less than 0.5. When initial density is above the density threshold, generally vehicles need more fuel consumption to run through the ring road in comparison with the case without tunnel. But the situation is just the opposite for larger normalized initial density such as 0.5.

## Keywords

Freeway tunnel effects, travel time, two-lane traffic model, lane-changing, weighted essentially non-oscillatory scheme

## 1. Introduction

A brief literature review has been reported by Hu et al.,<sup>1</sup> where the concluding remarks of several studies,<sup>2–5</sup> such as to reduce congestion at sags, a potentially highly effective and innovative way can be implemented using cooperative adaptive cruise control systems,<sup>3</sup> can be sought.

Some macroscopic considerations for multi-lane traffic flow dynamics were reported by Michalopoulos et al.<sup>6</sup> A multi-lane traffic model was proposed by Chang and Zhu<sup>7</sup> to analyze the dynamic traffic properties of a freeway segment under a lane-closure operation that often incurs complex interactions between mandatory lane-changing cars and traffic at unblocked lanes. A macroscopic behavior theory of traffic dynamics for homogeneous multi-lane freeways was developed by Daganzo,<sup>8</sup> which is shown to be qualitatively consistent with experimental observations, including puzzling. While recognizing that traffic flow is usually associated with aggressive and timid drivers, predictions for separate groups of lanes were made. Building

on continuum macroscopic behavior theory and focusing on the onset of congestion, the behavior of multi-lane freeway traffic past on ramps was further examined.<sup>9</sup> A two-lane model was proposed by Tang et al.,<sup>10</sup> in which the lane-changing model is consistent with car-following behavior on a two-lane freeway, with another multi-lane traffic

<sup>1</sup>Faculty of Engineering Science, University of Science and Technology of China (USTC), China

<sup>2</sup>School of Information Science and Technology, University of Science and Technology of China (USTC), China

<sup>3</sup>Faculty of Mechanics and Mathematics, Lomonosov Moscow State University, Russia

### Corresponding authors:

M N Smirnova, Faculty of Mechanics and Mathematics, Lomonosov Moscow State University, Moscow 119992, Russia.  
Email: wonrims@inbox.ru

Zuojin Zhu, Faculty of Engineering Science, University of Science and Technology of China (USTC), Hefei 230026, China.  
Email: zuojin@ustc.edu.cn

flow model accounting for lane width, lane-changing, and the number of lanes reported by Tang et al.<sup>11</sup> A multi-lane traffic model was proposed by Smirnova et al.,<sup>12</sup> in which they derived an expression for describing the acceleration component in the orthogonal direction in relation to lane changing.

Recently, a macroscopic traffic flow model that includes driver sensitivity to the number of free spaces ahead has been developed by Pour and Nassiri,<sup>13</sup> a multiclass multi-lane model for freeway traffic mixed with connected automated vehicles and regular human-piloted vehicles has been proposed by Pan et al.<sup>14</sup> In addition, some research results relating to microscopic multi-lane traffic modeling have been reported in previous studies.<sup>15–17</sup>

For lane changing, literature review was conducted by Zheng,<sup>18</sup> who reported several modules of lane-changing, such as the multi-lane kinematic wave module developed by Laval and Daganzo,<sup>19</sup> and the approach to extend kinematic wave theory proposed by Jin.<sup>20,21</sup> The present lane-changing model adopts a single parameter  $\beta_*$  not validated by real data, but simple and provides an approach in modeling this difficult traffic phenomenon: lane-changing being a primary trigger of oscillations,<sup>22</sup> with negative impact on traffic breakdowns and bottleneck discharge rate reduction at the onset of congestion.<sup>23</sup>

To make approximation of several widely applied macroscopic traffic flow models, numerical approach was given by Delis et al.,<sup>24</sup> briefly presenting the class of relaxation models introduced by Jin and Xin<sup>25</sup> and the family of spatial discretizations, that includes a second-order monotone upwind-centered scheme for conservation laws (MUSCL) and another WENO5 scheme improved by Borges et al.<sup>26</sup>

Recently, recognizing the need to effectively manage emerging autonomous vehicles (AV) flows in contending with daily recurrent congestion, Rao et al.<sup>27</sup> have developed a systematic procedure for understanding the impacts of AV flows on traffic conditions under different AV behavioral mechanisms (i.e., car-following and lane-changing) and different penetration rates. It was found that the presence of AV flows, depending on their adopted behavioral mechanisms, may have significant (either positive or negative) impacts on the overall traffic conditions. Furthermore, to evaluate the difference in the results of open and closed boundary simulations in heterogeneous non-lane-based traffic, a study of cellular automata (CA) simulation model has been carried out by Singh and Rao.<sup>28</sup> To evaluate the navigation performance of the Three Gorges–Gezhouba Dams (TGGD) for ship traffic, using multi-agent and discrete-event modeling theories, a data- and event-driven hybrid simulation model has been developed by Zhang et al.<sup>29</sup>

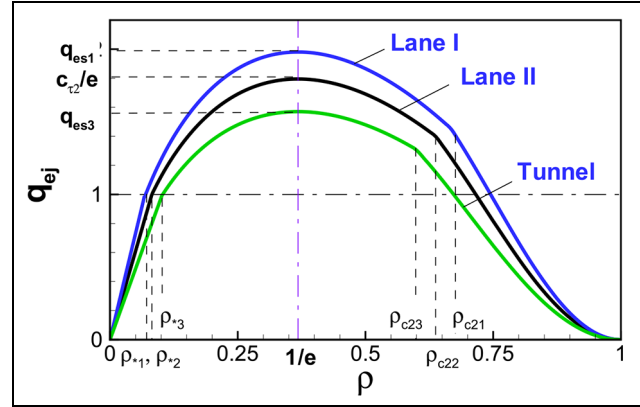


**Figure 1.** Fundamental diagram (FD) for traffic flows on a two-lane road with a tunnel.  $\rho$  is measured by jam density  $\rho_m$ , flow rate has the unit of  $q_0 = \rho_m v_0$ , and  $q_{esj} = c_{tj}/e \cdot [\rho_{*j} v_{fj} / \rho_{*2} v_{f2}]$ ,  $j = 1, 2$ , and 3 respectively for the equilibrium flow rates on the two lanes in normal road segment, and the equilibrium flow rate on a lane in the tunnel.

In this paper, in order to explore freeway tunnel effects on traffic flow as a task for the project of National Natural Science Foundation of China, a two-lane traffic model (TLM) is put forward. The freeway has a tunnel with a length of 0.3 km and a speed limit of 80 km/h. Free flow speeds on lanes I and II are 120 and 100 km/h, respectively. One major difficulty involves describing the net lane-changing rate more conveniently and appropriately. Hence, TLM proposes a lane-changing model with lane-changing time to describe the net lane-changing rate. TLM further uses free flow speed and second critical speed to determine the fundamental diagram (FD) as done by Kiselev et al.<sup>30</sup> and assumes that in freeway tunnel the speed limit is just the free flow speed, as shown in Figure 1. In the numerical simulation based on TLM, using time-averaged grid speed of traffic flow and car-performance diagram, the vehicle fuel consumption can be calculated.

With the aim to ascertain freeway tunnel effects on traffic flow, a simulation platform is built with TLM, where the key difficulty is how to solve TLM equations more accurately. Hence, a third-order Runge–Kutta method<sup>31,32</sup> is used to handle the time derivative term, and a fifth-order weighted essentially non-oscillatory scheme developed<sup>33,34</sup> to calculate numerical flux. To validate TLM, some distributions of the time-averaged traffic speed near the tunnel are compared with the speed curves recorded at Kobotoke tunnel in Japan reported by Koshi et al.<sup>35</sup> and the calculated speed on the basis of a behavioral kinematic wave model developed by Jin.<sup>36</sup>

It is noted that in comparison with existing modules of lane-changing, the present lane-changing module is possibly the simplest. Numerical results show that under

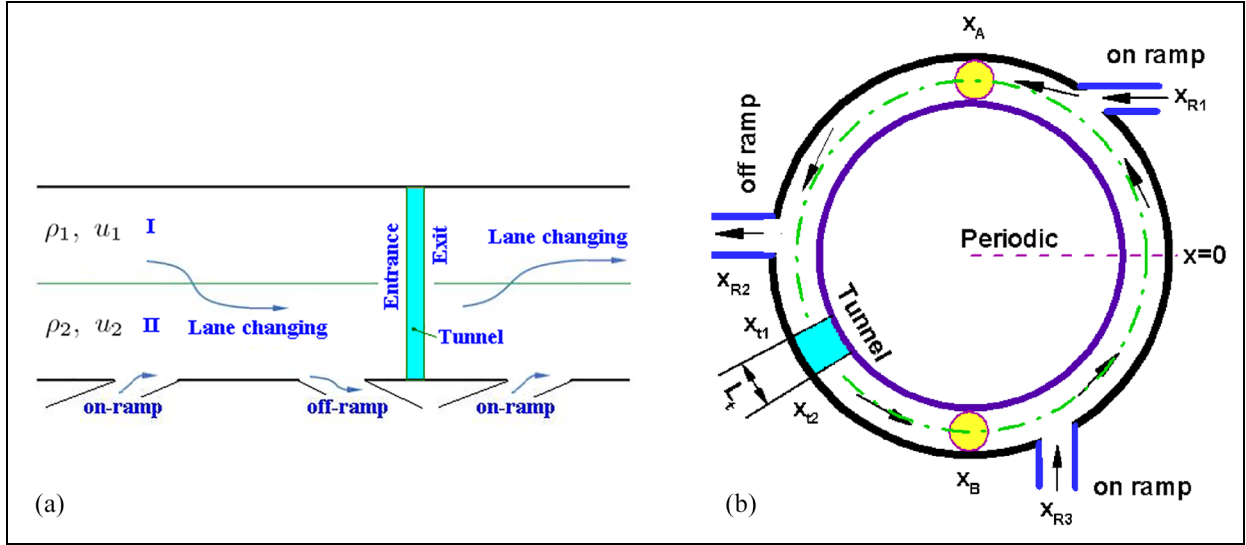


**Figure 2.** (a) Illustration of a two-lane traffic flow and (b) schematic diagram of ring traffic flow with a tunnel and two initial jams at  $X_I (I = A, B)$ .

The tunnel entrance and exit are, respectively, located at  $X_{t1}$  and  $X_{t2}$ .

conditions of traffic flow simulation in this paper, when the freeway tunnel length is 0.3 km, if there is a tunnel triggered traffic shock and the initial density normalized by jam density is less than 0.5, the mean tunnel travel time is approximately 0.0125 h, suggesting that the mean traffic flow speed in the tunnel is around 24 km/h. There is a density threshold of shock formation, which can be determined by examining the spatiotemporal evolution of traffic density on the freeway. Such a threshold depends on the off-ramp flow just upstream the tunnel. When initial density is above the density threshold of shock formation, tunnel affects the vehicle fuel consumption significantly. Generally, vehicles need more fuel consumption to run through the ring road in comparison with the case without tunnel. But for larger normalized initial density such as 0.5, the opposite is true.

In this paper, TLM equations are presented before the numerical method for solving TLM equations and then extensive numerical results are discussed, with some conclusions provided finally.

## 2. TLM equations

Different from previous multi-lane traffic modeling given in the foregoing section, to avoid mathematical complexity of modeling vehicular flow on a four-lane road, we adopt lane-changing time to describe the net lane-changing rate.

Consider Figure 2(a), which shows two lanes labeled by I, II, having traffic densities  $\rho_1, \rho_2$  and traffic speeds  $u_1, u_2$ . While lane changing of cars is allowed, generally cars on lane I have a higher free flow speed than those on lane II. However, if the cars are in the tunnel, the free flow

speed on any lane is assumed to be the speed limit of the tunnel. As shown schematically in Figure 2(b), the freeway is a ring type with two initial jams at  $X_I, I = A, B$ , and the tunnel with a length  $L_t$  has an entrance located at  $X_{t1}$  just downstream of the off-ramp intersection at  $X_{R2}$ . Cars on ramp runs into or off the main road through the three intersections connected with the lane IV at  $X_{R1}, X_{R2}$ , and  $X_{R3}$ . Any vehicle attempting to run off the main road should at first make lane changes and shift onto lane II. Lane-changing occurs spontaneously to keep local homogeneity of vehicular distribution, irrespective of whether it is mandatory or discretionary.

To describe the two-lane traffic flow, traffic densities,  $\rho_1$  and  $\rho_2$  and corresponding flow rates  $q_1 (= \rho_1 u_1)$  and  $q_2 (= \rho_2 u_2)$  are taken as the main variables. Labeling the lane average density  $\rho = (\rho_1 + \rho_2)/2$ , for cars on lane I expecting to shift onto lane II, its density should be  $(\rho_1 - \rho)$ . If the traffic relaxation times on lane I and II are  $\tau_1$  and  $\tau_2$ , then the lane average relaxation time is  $\tau = (\tau_1 + \tau_2)/2$ , assuming that vehicular lane-changing time is  $(\tau \beta_\star)$ , the net lane-changing rate on lane I ( $\rho_1$ ) could simply be approximated by  $-(\rho_1 - \rho)/(\tau \beta_\star)$ . Therefore, using the randomly generated ramp parameter  $\sigma$  as reported by Zhang et al.,<sup>37</sup> TLM equations can be written as follows:

$$\begin{cases} \rho_{1t} + q_{1x} = -(\rho_1 - \rho)/(\tau \beta_\star), \\ u_{1t} + u_1 u_{1x} = R_1/\rho_1, \\ \rho_{2t} + q_{2x} = -(\rho_2 - \rho)/(\tau \beta_\star) + \sigma q_2/l_0, \\ u_{2t} + u_2 u_{2x} = R_2/\rho_2 \end{cases} \quad (1)$$

where  $R_1$  and  $R_2$  can be expressed as:<sup>38–40</sup>

$$\begin{cases} R_1 = (q_{1e} - q_1)/\tau_1 - p_{1x} + [\rho_1 v_1 u_{1x}]_x, \\ R_2 = (q_{2e} - q_2)/\tau_2 - p_{2x} + [\rho_2 v_2 u_{2x}]_x, \end{cases} \quad (2)$$

where  $l_0$  is the length scale of traffic flow. On lane  $l \in \{1, 2\}$ ,  $q_{le}$  and  $R_l/\rho_l$  are equilibrium flow rate and acceleration,  $v_l (= 2G_l\tau_l/\rho_l)$ ,  $G_l$  and  $\tau_l$  are traffic kinematic viscosity, modulus of elasticity and relaxation time, traffic pressure  $p_l = c_l^2\rho_l$ , and  $c_l$  is traffic sound speed.

To simulate ramp flow, TLM uses a random number  $\sigma$  provided by a random number generator with Gaussian normal distribution which takes the mean, variance, and number seed as dummy variables, adopts  $(\tau\beta_\star)$  to represent lane-changing time, whose time ratio to relaxation  $\tau$  is as follows:

$$\beta_\star = \begin{cases} \infty, & |\rho_1 - \rho_2| < 1 \text{ veh/km}, \\ \rho_2/\rho_1 & \text{otherwise,} \end{cases} \quad (3)$$

which indicates that when the absolute value of traffic densities between the two lanes is below 1 veh/km, vehicular drivers have not made any attempt to carry out lane-changing whether mandatory or discretionary; otherwise, it is assumed to be the density ratio  $\rho_2/\rho_1 \approx 1$ . In comparison with modules of existing lane-changing, the present module is possibly the simplest. According to car driving experience, the assumption of lane-changing time is reasonable.

In normal road segment out of tunnels, cars have different free flow speed and braking distance on different lanes, indicating that equilibrium traffic flow rate is lane-dependent, as shown in Figure 1. Let jam density be  $\rho_m$ , the equilibrium traffic flow rate can be written as:<sup>37</sup>

$$q_{el} = \begin{cases} \rho_l v_{fj}, & \text{for } \rho_l \leq \rho_{*l}; \\ -c_{\tau l} \rho_l \ln(\rho_l/\rho_m), & \text{for } \rho_{*l} < \rho_l \leq \rho_{c2l}; \\ B_l \rho_l \{1 - \text{sech}[\Lambda_l \ln(\rho_l/\rho_m)]\}, & \text{for } \rho_{c2l} < \rho_l \leq \rho_m, \end{cases} \quad (4)$$

where subscript  $j$  is dependent on road conditions (schematically shown in Figure 2(b)): in the normal road segment,  $j = l = 1$ , and 2, representing the corresponding variables of cars on lane I, II; while in the tunnel,  $j = 3$ , representing the relevant variables of all cars under the tunnel speed limit.

At second critical density  $\rho_{c2}$ , traffic flow has an equilibrium speed  $u_{c2}$ . Defining a speed ratio  $\Lambda_l = c_{\tau l}/u_{c2}$ , the parameter  $B_l$  can be written as:

$$B_l = u_{c2}/\{1 - \text{sech}[\Lambda_l \ln(\rho_{c2l}/\rho_m)]\}. \quad (5)$$

$c_{\tau l}$  is the traffic saturation speed at the density  $(\rho/\rho_m = 1/e)$ , it is calculated by:

$$c_{\tau l} = v_{fj}/\ln[1 + X_{brl}/l], \quad (6)$$

where  $l$  is average length of cars, and  $X_{brl}$  is the braking distance. As the expressions of traffic pressure and sound

speed are also similar to that reported in Zhang et al.,<sup>41</sup> we will not repeat again.

### 3. Numerical method

To solve TLM equations, the time derivative term is treated with the third-order Runge–Kutta scheme,<sup>31,32</sup> and numerical flux is calculated by the fifth-order weighted essentially non-oscillatory scheme (WENO5).<sup>33,34</sup> As details of the right and left characteristic matrices are crucial in building the platform of simulation, we will show the expressions of matrix elements explicitly in this section.

The traffic pressure gradient  $p_{lx}$  is given by:

$$p_{lx} = c_l^2 \rho_{lx}.$$

Using  $R_{1*} = R_1 + p_{1x} - (\rho_1 - \rho)u_1/(\tau\beta_\star)$  instead of  $R_1$ , and  $R_{2*} = R_2 + p_{2x} - (\rho_2 - \rho)u_2/(\tau\beta_\star) + \sigma q_2 u_2/l_0$  instead of  $R_2$ , the governing Equations (1) and (2) can be written as:

$$\frac{\partial \mathbf{U}}{\partial t} + \frac{\partial \mathbf{F}(\mathbf{U})}{\partial x} = \mathbf{S}, \quad (7)$$

where  $\mathbf{U} = (\rho_1, q_1, \rho_2, q_2)^T$ ,  $\mathbf{F}(\mathbf{U}) = (q_1, q_1^2/\rho_1 + p_1, q_2, q_2^2/\rho_2 + p_2)^T$ , and  $\mathbf{S} = [(\rho_2 - \rho)/(\tau\beta_\star), R_{1*}, 0, (\rho_1 - \rho)/(\tau\beta_\star) + \sigma q_2/l_0, R_{2*}]^T$ , with superscript ‘ $T$ ’ representing vector transpose.

The eigenvalues of Equation (7)  $a_k$ , ( $k = 1, 2, \dots, 4$ ) may be expressed as  $a_1 = u_1 - c_1$ ,  $a_2 = u_1 + c_1$ , and  $a_3 = u_2 - c_2$ ,  $a_4 = u_2 + c_2$  where the Jacobian matrix is

$$\mathbf{A} = \begin{pmatrix} a_{11} & a_{12} & a_{13} & a_{14} \\ a_{21} & a_{22} & a_{23} & a_{24} \\ a_{31} & a_{32} & a_{33} & a_{34} \\ a_{41} & a_{42} & a_{43} & a_{44} \end{pmatrix} = \begin{pmatrix} 0 & 1 & 0 & 0 \\ -u_1^2 + c_1^2 & 2u_1 & 0 & 0 \\ 0 & 0 & 0 & 1 \\ 0 & 0 & u_2^2 - c_2^2 & 2u_2 \end{pmatrix}. \quad (8)$$

Let the eigenvalues, the left and right eigenvectors be

$$a_k, \quad \mathbf{l}_k, \quad \mathbf{r}_k, \quad k \in \{1, 2, 3, 4\}, \quad (9)$$

then the Jacobian matrix  $\mathbf{A}$  can be written as follows:

$$\mathbf{A} = \mathbf{R}\mathbf{a}\mathbf{L}, \quad \mathbf{L} = \mathbf{R}^{-1}, \quad (10)$$

where  $\mathbf{a} = \text{diag}(a_1, a_2, a_3, a_4)$  is a diagonal matrix composed of eigenvalues;  $\mathbf{R}$ ,  $\mathbf{L}$  are respectively right and left characteristic matrices composed of relevant eigenvectors:

$$\mathbf{R} = [\mathbf{r}_1, \mathbf{r}_2, \mathbf{r}_3, \mathbf{r}_4], \quad \mathbf{L} = \begin{bmatrix} \mathbf{l}_1 \\ \mathbf{l}_2 \\ \mathbf{l}_3 \\ \mathbf{l}_4 \end{bmatrix}. \quad (11)$$

The approach of deriving the elements of  $\mathbf{R}$  is similar to that described by Zhu and Wu.<sup>42</sup> It is characterized by assuming the  $k$ th element of vector  $\mathbf{r}_k$  to be unity, i.e.,  $r_{kk} = 1$ , for  $k \in \{1, 2, 3, 4\}$ . As the Jacobian matrix  $\mathbf{A}$  has a special structure with 10 zero elements, using the assumption  $r_{kk} = 1$ , one obtains

$$\mathbf{R} = \begin{pmatrix} r_{11} & r_{12} & 0 & 0 \\ r_{21} & r_{22} & 0 & 0 \\ 0 & 0 & r_{33} & r_{34} \\ 0 & 0 & r_{43} & r_{44} \end{pmatrix}, \quad \mathbf{L} = \begin{pmatrix} l_{11} & l_{12} & 0 & 0 \\ l_{21} & l_{22} & 0 & 0 \\ 0 & 0 & l_{33} & l_{34} \\ 0 & 0 & l_{43} & l_{44} \end{pmatrix} \quad (12)$$

From Equation (8), it is seen that  $a_{ij} = 0$ , for  $i = 1, 2$  and  $j = 3, 4$ ; or  $i = 3, 4$  and  $j = 1, 2$ . Hence we have

$$\begin{aligned} \begin{pmatrix} r_{11} & r_{12} \\ r_{21} & r_{22} \end{pmatrix} &= \begin{pmatrix} 1 & -\frac{a_{22}-a_2}{a_{21}} \\ -\frac{a_{11}-a_1}{a_{12}} & 1 \end{pmatrix}, \quad \begin{pmatrix} r_{33} & r_{34} \\ r_{43} & r_{44} \end{pmatrix} \\ &= \begin{pmatrix} 1 & -\frac{a_{44}-a_4}{a_{43}} \\ -\frac{a_{33}-a_3}{a_{34}} & 1 \end{pmatrix} \end{aligned} \quad (13)$$

and

$$\begin{aligned} \begin{pmatrix} l_{11} & l_{12} \\ l_{21} & l_{22} \end{pmatrix} &= \frac{1}{1 - r_{12}r_{21}} \begin{bmatrix} 1 & -r_{12} \\ -r_{21} & 1 \end{bmatrix}, \\ \begin{pmatrix} l_{33} & l_{34} \\ l_{43} & l_{44} \end{pmatrix} &= \frac{1}{1 - r_{34}r_{43}} \begin{bmatrix} 1 & -r_{34} \\ -r_{43} & 1 \end{bmatrix}. \end{aligned} \quad (14)$$

These explicit expressions of elements for characteristic matrices  $\mathbf{R}$  and  $\mathbf{L}$  in Equations (12)–(14) largely decrease the complexity in building simulation platform with TLM model.

The details of calculation of the numerical flux with the WENO5 scheme have been reported by Zhang et al.,<sup>43</sup> and it is unnecessary to repeat here. For the convenience of the description of a third-order Runge–Kutta scheme,<sup>31,32</sup> labeling

$$\mathcal{L}(\mathbf{U}) = -\frac{\partial \mathbf{F}(\mathbf{U})}{\partial \mathbf{x}} + \mathbf{S}, \quad (15)$$

so that

$$\mathcal{L}(\mathbf{U}_i) = -\frac{\hat{\mathbf{F}}_{i+1/2} - \hat{\mathbf{F}}_{i-1/2}}{\Delta x} + \mathbf{S}_i, \quad (16)$$

with the numerical flux  $\hat{\mathbf{F}}_{i+1/2}$  predicted by the WENO5 scheme, to seek the numerical solution of

$$\frac{\partial \mathbf{U}}{\partial t} = \mathcal{L}(\mathbf{U}), \quad (17)$$

we have the form of the third-order Runge–Kutta scheme

$$\begin{cases} \mathbf{U}_i^{(1)} = \mathbf{U}_i^n + \Delta t \mathcal{L}(\mathbf{U}_i^n), \\ \mathbf{U}_i^{(2)} = (3\mathbf{U}_i^n + \mathbf{U}_i^{(1)})/4 + \Delta t \mathcal{L}(\mathbf{U}_i^{(1)})/4, \\ \mathbf{U}_i^{n+1} = (\mathbf{U}_i^n + 2\mathbf{U}_i^{(2)})/3 + 2\Delta t \mathcal{L}(\mathbf{U}_i^{(2)})/3, \end{cases} \quad (18)$$

where the superscript  $n$  denotes time level.

Labeling  $\omega = \Delta t / \Delta x$ , the Courant–Friedrichs–Lewy (CFL) condition of the numerical method is

$$C_{FL} = \omega \cdot \max |a_{k,i}| < 1, \quad k \in \{1, 2, 3, 4\}; \quad (19)$$

$$i = 0, 1, 2, \dots, I_{\max} - 1$$

where  $a_{k,i}$  represents the  $k$ th eigenvalue for  $\mathbf{A}$  at  $x_i$ ,  $I_{\max}$  is the maximum number of mesh, and the Courant number  $C_{FL}$ <sup>44</sup> is fixed at 0.6 to ensure numerical stability.

## 4. Results and discussion

### 4.1. Simulation parameters

The freeway tunnel has a speed limit  $v_{f3}$  ( $= 80$  km/h), as shown in Table 1. The value is based on the view of car drivers traveling freeway tunnels in China. As shown in the first column of Table 1, free flow speeds on lanes I, II are  $v_{f1} = 120$  and  $v_{f2} = 100$  km/h; the corresponding relaxation times are 6.735 and 9.007 s, with the relaxation time within tunnel being 12.834 s. In the second column of Table 1, three ramp intersections are fixed at  $X_{R1} = 12$  km,  $X_{R2} = 45$  km, and  $X_{R3} = 78$  km. While in the third column, the entrance of the tunnel is fixed at  $X_{t1} = 65$  km, the tunnel length is taken as  $L_t = 0.3$  km, and the tunnel exit is at  $X_{t2} = 65.3$  km. In comparing with the two speed trajectories recorded at the Kobotoke in Japan as reported by Koshi et al.,<sup>24</sup> the length of tunnel is taken as 1.5 km. [AQ: 1] The total length of the ring freeway is  $L = 100$  km. In the numerical tests, the second critical speed  $u_{c2}$  is set as 18 km/h, and Reynolds number for the vehicular flow  $Re = l_0 v_0 / \nu$  is set as 64. Two initial jams are assumed to be located at  $X_I$ , ( $I = A, B$ ), other traffic flow parameters, such as the first and second critical densities  $\rho_{*j}$  and  $\rho_{c2j}$ ,  $j = 1, 2, 3$ , can also be seen in Table 1. The parameters of random number generator for ramp flows are shown in Table 2.

In the numerical simulation of ring road vehicular flow as shown in Figure 2, the FDs are shown in Figure 1. The initial density is assumed to be

**Table 1.** Parameters of traffic flow on ring road.

$v_{f1}$ (km/h)	120	$\rho_{*1}$	0.0676	$X_{t2}$ (km)	65.3
$v_{f2}$ (km/h)	100	$\rho_{*2}$	0.0819	$L_t^c$ (km)	0.3
$v_{f3}$ (km/h)	80	$\rho_{*2}$	0.1021	$\rho_m$ (veh/km)	172
$X_{br1}$ (m)	80	$\rho_{c21}$	0.6676	$l$ (m)	5.8
$X_{br2}$ (m)	65	$\rho_{c22}$	0.6374	$l_0$ (m)	100
$X_{br3}$ (m)	51	$\rho_{c23}$	0.5984	$v_0 = \rho_{*2} v_{f2}$ (m/s)	2.2756
$c_{\tau 1}$	5.437	$X_{R1}$ (km)	12	$t_0$ (s)	43.945
$c_{\tau 2}$	4.879	$X_{R2}$ (km)	45	$L$ (km)	100
$c_{\tau 3}^a$	4.280	$X_{R3}$ (km)	78	$l_{max}$	1001
$\tau_1$ (s)	6.735	$X_A$ (km)	25		
$\tau_2$ (s)	9.007	$X_B$ (km)	75		
$\tau_3$ (s)	12.834	$X_{t1}$ (km)	65		

<sup>a</sup> $c_{\tau j}, j = 1, 2, 3$  are measured by  $v_0$ . <sup>b</sup> $\rho_{c2j}, \rho_{*j}$  are measured by  $\rho_m$ . <sup>c</sup>Tunnel length  $L_t = X_{t2} - X_{t1}$ .

**Table 2.** Parameters of random number generator for ramp flows.

Case	$\sigma_{1av}$	$\sigma_{2av}$	$\sigma_{3av}$	$\sigma'_1 = \sigma'_2 = \sigma'_3$
RF0	0	0	0	0
RF1	0.03	-0.06	0.03	0.003
RF2	0.06	-0.12	0.06	0.003
RF3	0.09	-0.18	0.09	0.003
RF4	0.12	-0.24	0.12	0.003

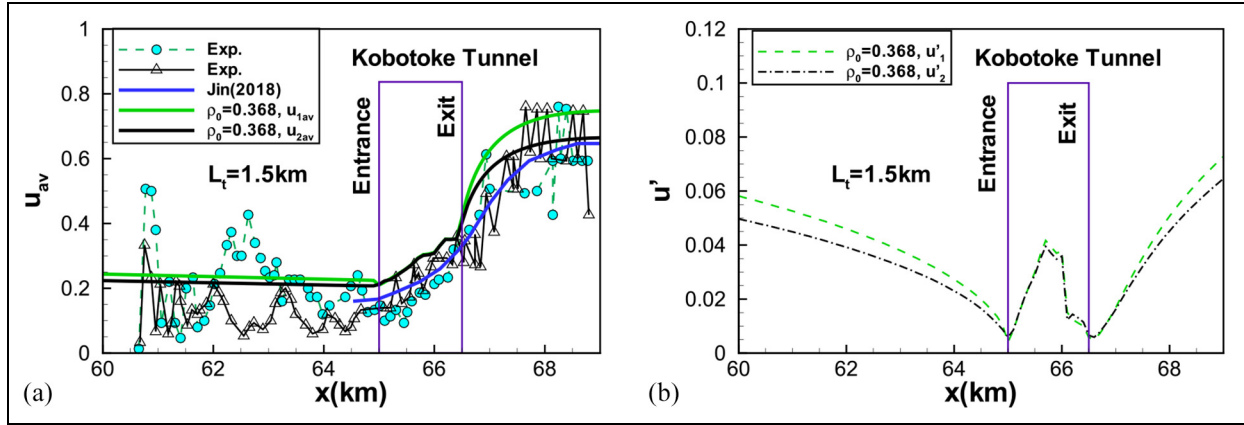


**Figure 3.** Comparison of time-averaged speed  $u_{av}$  for  $\rho_0 = 0.368$  with existing data, with corresponding rms value  $u'_i$  [AQ: 2] The two speed trajectories with legend “Exp” are recorded at the Kobotoke tunnel in Japan;<sup>35</sup> the calculated speed labeled by the blue solid curve with unfilled purple squares are extracted from Jin,<sup>36</sup> normalized by  $v_{f2}$ .

$$\left. \begin{aligned} \rho_1(0, x) &= \begin{cases} 1, & \text{for } x \in [x_I - 1/2, x_I + 1/2], \\ \rho_0, & \text{otherwise.} \end{cases} \\ \rho_2(0, x) &= \begin{cases} 1, & \text{for } x \in [x_I - 1/2, x_I + 1/2], \\ 1.125\rho_0, & \text{otherwise.} \end{cases} \end{aligned} \right\} \quad (20)$$

with  $q(0, x) = q_e(\rho(0, x))$ . We have assumed that the density on lane II is slightly higher than on lane I, so that lane-changing can occur. The initial jam propagation depends

closely on the value of  $\rho_0$ , tunnel effects, ramp flows, and traffic elasticity  $\gamma$  as reported in Smirnova et al.<sup>45,46</sup>

#### 4.2. Model comparison

Resetting the tunnel length as  $L_{tu} = 1.5$  km instead of 8 km, and the time-averaged speed  $u_{av}$  and its rms  $u'$  for  $\rho_0 = 0.368$  near the tunnel in the case without ramp effects are predicted and shown in Figure 3(a) and (b). For

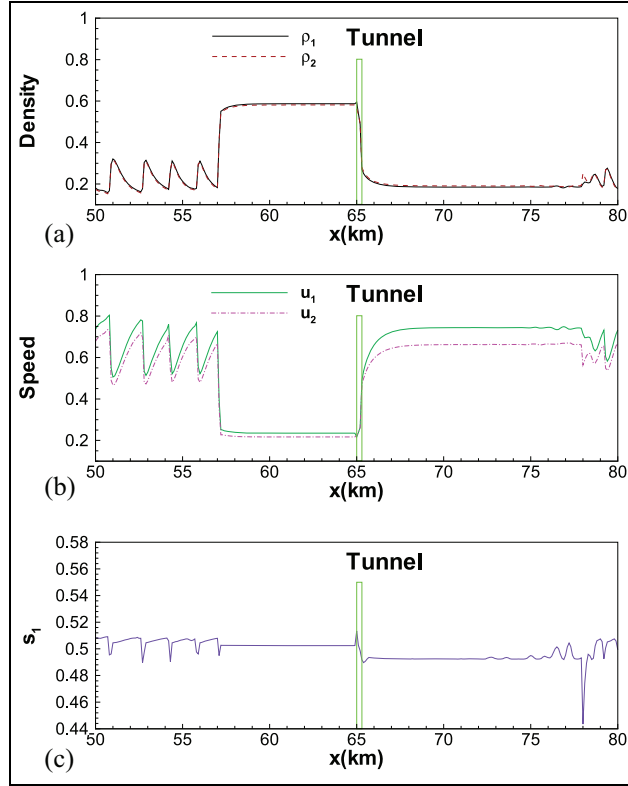


**Figure 4.** Distributions of (a) traffic density, (b) speed, and (c) density fraction  $s_1 [= \rho_1/(\rho_1 + \rho_2)]$  at  $t = 2$  h on the ring road for  $\rho_0 = 0.3$  in the case of RF4. [AQ: 3]

comparison, Figure 3(a), the observed speed data<sup>35</sup> and the calculated speed on the basis of a behavioral kinematic wave model developed by Jin<sup>36</sup> are illustrated. It can be seen that the predicted speeds shown by green and black coarse lines agree with the published data quite well, suggesting that the TLM is fairly reliable. As reported elsewhere,<sup>47</sup> indeed, this comparison is used just to indicate TLM has its practical reasonability. How much is the uncertainty of the average speed is not crucial as the traffic flow conditions are naturally different.

### 4.3. Variable distributions

The distributions of traffic density  $\rho_l$  and speed  $u_l$ ,  $l \in \{1, 2\}$  are shown in Figure 4(a) and (b), with the tunnel illustrated by a solid square. As a result of traffic shock formation at the tunnel entrance, at time  $t = 2$  h, traffic density in the segment close to tunnel entrance is higher, but speed is correspondingly lower. In Figure 4(c), the density fraction on lane I  $s_1$  is illustrated. From Equation (1), the equation of  $s_1$  can be expressed in the form

$$\begin{aligned} \frac{\partial s_1}{\partial t} + \frac{1}{\rho_1 + \rho_2} \left[ (1 - s_1) \frac{\partial q_1}{\partial x} - s_1 \frac{\partial q_2}{\partial x} \right] \\ = \frac{1/2 - s_1}{\tau \beta_\star} - s_1 \sigma \frac{q_2/l_0}{\rho_1 + \rho_2}, \end{aligned}$$

showing that time variation of  $s_1$  has one source term  $(1/2 - s_1)/(\tau \beta_\star)$ , implying that the desired value of density fraction is  $1/2$ , while the another source term  $-s_1 \sigma q_2/l_0/(\rho_1 + \rho_2)$  indicates ramp-flow effects. It also depends on the term relating to gradients of flow rates on the left hand side of  $s_1$ -equation.

For the case of  $\rho_0 = 0.3$ , at the time of  $t = 2$  h, it can be seen that in the freeway tunnel traffic density drops rapidly at first from a value about 0.6 at the tunnel entrance to a value about 0.27 at the tunnel exit. In the downstream segment close to the tunnel exit, traffic density drops rapidly at first from 0.27 to about 0.19 within a distance of about 1 km and maintains the value within a segment distance of about 12 km, indicating that the tunnel provides a smooth downstream segment close to the tunnel exit if there is a traffic shock at the tunnel entrance.

### 4.4. Travel time

As every traveler expects to arrive at a destination without travel delay, travel time is an important factor of consideration. Different from the study of Chang and Mahmassani,<sup>48</sup> in which rules were proposed for describing urban commuters' predictions of travel time as well as adjustments of departure time in response to unacceptable arrivals in their daily travel under limited information, as well as different from the method reported by Wang et al.,<sup>49</sup> they estimated the travel time using a regression model, but in this paper, the mean travel time through the freeway loop (called as mean travel time) as well as the mean travel time through the tunnel (called as tunnel mean travel time) are calculated using grid traffic speed  $u_i(t)$ , similar to that reported elsewhere by Zhang et al.<sup>43</sup>

In the case without ramp effects, the  $\rho_0$ -dependencies of mean travel time  $T_{t,av}$  and tunnel mean travel time  $T_{tu,av}$  are shown in Figure 5(a) and (b).  $T_{t,av}$  through lane I is lower than that through lane II, as the free flow speed on lane I is assumed to be 120 km/h, slightly higher than the free flow speed of 100 km/h on lane II. The freeway tunnel has brought about a short travel delay when the traffic shock is triggered at the tunnel entrance, as shown in Table 3 and Figure 5(b). For instance, when  $\rho_0 = 0.368$ , the travel delay on lane I and II are, respectively, 7.314 and 6.96 min. When  $\rho_0$  is below the density threshold of traffic shock formation ( $\rho_{th} \approx 0.2$ ),  $T_{tu}$  manifests a plateau with a height of about 0.0125 h for  $\rho_0 \in [0.2, 0.5]$ ,

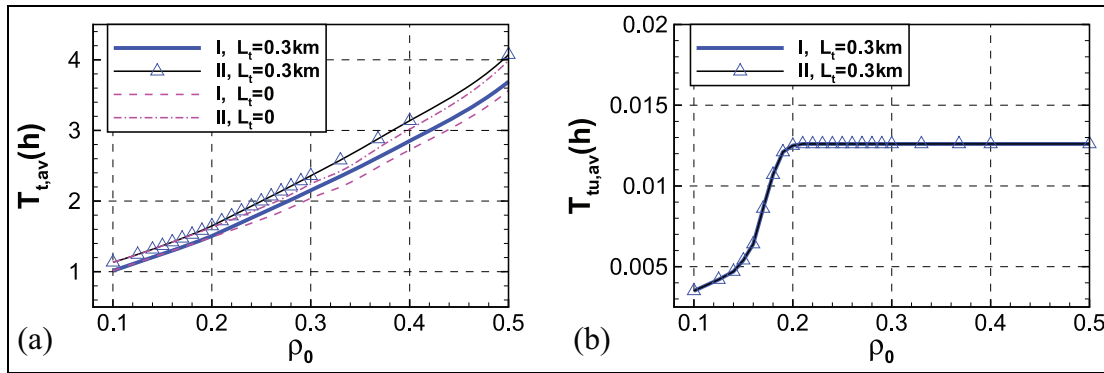


**Figure 5.** Density dependencies of (a) mean travel time  $T_{t,av}$  and (b) tunnel mean travel time  $T_{tu,av}$  in the case without ramp effects.

**Table 3.** Distributions of  $T_{t,av}$ ,  $T_{tu,av}$  without ramp effects. [AQ: 4]

$L_t = 0.3$					$L_t = 0$			
I		II			I		II	
$\rho_0$	$T_{t,av}$ (h)	$T_{tu,av}$ (h)						
0.1	1.0141	0.0035	1.1332	0.0037	1.0137	0.0000	1.1351	0.0000
0.125	1.1322	0.0042	1.2436	0.0043	1.1312	0.0000	1.2430	0.0000
0.14	1.2037	0.0047	1.3174	0.0047	1.2020	0.0000	1.3159	0.0000
0.15	1.2514	0.0054	1.3684	0.0054	1.2499	0.0000	1.3675	0.0000
0.16	1.2995	0.0064	1.4202	0.0062	1.2975	0.0000	1.4187	0.0000
0.17	1.3484	0.0086	1.4730	0.0083	1.3453	0.0000	1.4702	0.0000
0.18	1.3976	0.0107	1.5270	0.0103	1.3931	0.0000	1.5219	0.0000
0.19	1.4479	0.0121	1.5826	0.0119	1.4410	0.0000	1.5744	0.0000
0.2	1.5052	0.0125	1.6476	0.0124	1.4895	0.0000	1.6276	0.0000
0.21	1.5693	0.0126	1.7180	0.0124	1.5383	0.0000	1.6814	0.0000
0.22	1.6331	0.0126	1.7877	0.0124	1.5876	0.0000	1.7358	0.0000
0.23	1.6972	0.0126	1.8581	0.0124	1.6371	0.0000	1.7911	0.0000
0.24	1.7610	0.0126	1.9279	0.0124	1.6879	0.0000	1.8473	0.0000
0.25	1.8253	0.0126	1.9980	0.0124	1.7396	0.0000	1.9048	0.0000
0.26	1.8896	0.0126	2.0685	0.0124	1.7914	0.0000	1.9627	0.0000
0.27	1.9534	0.0126	2.1384	0.0124	1.8476	0.0000	2.0244	0.0000
0.28	2.0182	0.0126	2.2102	0.0124	1.9102	0.0000	2.0954	0.0000
0.29	2.0847	0.0126	2.2842	0.0124	1.9737	0.0000	2.1673	0.0000
0.3	2.1515	0.0126	2.3586	0.0124	2.0395	0.0000	2.2421	0.0000
0.33	2.3507	0.0126	2.5794	0.0124	2.1993	0.0000	2.4234	0.0000
0.368	2.6155	0.0126	2.8800	0.0124	2.4799	0.0000	2.7490	0.0000
0.4	2.8516	0.0126	3.1372	0.0124	2.7248	0.0000	3.0171	0.0000
0.5	3.6911	0.0126	4.0727	0.0125	3.5654	0.0000	3.9915	0.0000

suggesting that the mean flow speed in the freeway tunnel is around 24 km/h. Obviously, the tunnel mean travel time  $T_{tu,av}$  has a turning point, at the density threshold for traffic shock formation  $\rho_{th}$ . However, as soon as the turning point is crossed,  $T_{tu,av}$  approaches to a constant value.

In the case with ramp effects, when ramp parameters are assigned in the cases of RF1 and RF4 (see Table 2), density dependencies of mean travel time  $T_{t,av}$  and tunnel mean travel time  $T_{tu,av}$  are shown in Figure 6(a) and (b).

Figure 6(a) shows that the travel time deviation due to different assignments of ramp parameters is rather small, as can be seen in Table 4. When  $\rho_0 = 0.26$ , as a result of increasing mean parameters of on/off ramp flows, the travel time delay through lane I is about 2.5 s, with a delay through lane II of 35.3 s, both within 1 min. However, Figure 6(b) indicates that the turning point of mean tunnel travel time has increased from  $\rho_{th} = 0.2$  to  $\rho_{th} = 0.23$ , as seen in Table 5.

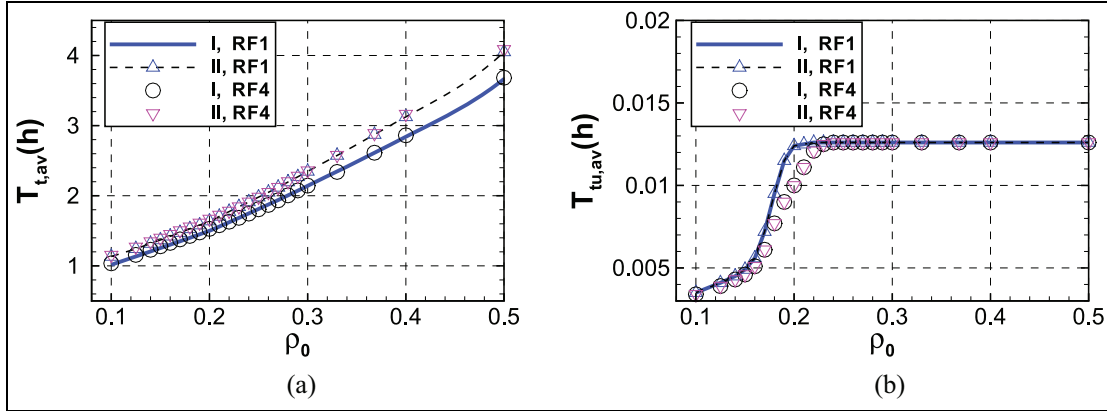


**Figure 6.** Density dependencies of (a) mean travel time  $T_{t,av}$  and (b) tunnel mean travel time  $T_{tu,av}$  for tunnel length  $L_{tu} = 0.3$  km in the cases of RFI and RF4.

**Table 4.** Distributions of  $T_{t,av}$ ,  $T_{tu,av}$  for  $L_t = 0.3$  km with ramp effects.

RFI					RF4				
I		II			I		II		
$\rho_0$	$T_{t,av}$ (h)	$T_{tu,av}$ (h)							
0.1	1.0160	0.0035	1.1339	0.0037	1.0359	0.0034	1.1534	0.0036	
0.125	1.1345	0.0041	1.2443	0.0042	1.1569	0.0039	1.2694	0.0040	
0.14	1.2055	0.0045	1.3183	0.0046	1.2300	0.0043	1.3457	0.0044	
0.15	1.2532	0.0049	1.3696	0.0049	1.2792	0.0046	1.3974	0.0047	
0.16	1.3019	0.0056	1.4219	0.0054	1.3279	0.0051	1.4503	0.0051	
0.17	1.3506	0.0072	1.4743	0.0070	1.3777	0.0061	1.5039	0.0060	
0.18	1.4002	0.0095	1.5275	0.0092	1.4274	0.0077	1.5578	0.0074	
0.19	1.4492	0.0115	1.5817	0.0112	1.4773	0.0090	1.6125	0.0087	
0.2	1.5007	0.0124	1.6391	0.0122	1.5280	0.0100	1.6684	0.0097	
0.21	1.5593	0.0125	1.7048	0.0124	1.5794	0.0111	1.7254	0.0108	
0.22	1.6220	0.0126	1.7740	0.0124	1.6307	0.0121	1.7829	0.0120	
0.23	1.6852	0.0126	1.8430	0.0124	1.6850	0.0125	1.8446	0.0124	
0.24	1.7478	0.0126	1.9116	0.0124	1.7453	0.0126	1.9125	0.0124	
0.25	1.8109	0.0126	1.9806	0.0124	1.8066	0.0126	1.9824	0.0124	
0.26	1.8737	0.0126	2.0494	0.0124	1.8696	0.0126	2.0505	0.0124	
0.27	1.9373	0.0126	2.1191	0.0124	1.9343	0.0126	2.1221	0.0124	
0.28	2.0055	0.0126	2.1958	0.0124	2.0061	0.0126	2.2037	0.0124	
0.29	2.0724	0.0126	2.2697	0.0124	2.0755	0.0126	2.2816	0.0124	
0.3	2.1415	0.0126	2.3467	0.0124	2.1436	0.0126	2.3578	0.0124	
0.33	2.3469	0.0126	2.5745	0.0124	2.3391	0.0126	2.5784	0.0124	
0.368	2.6108	0.0126	2.8727	0.0124	2.6134	0.0126	2.8892	0.0124	
0.4	2.8411	0.0126	3.1254	0.0124	2.8614	0.0126	3.1643	0.0124	
0.5	3.6655	0.0126	4.0507	0.0125	3.6833	0.0126	4.0871	0.0125	

#### 4.5. Density threshold of traffic shock formation

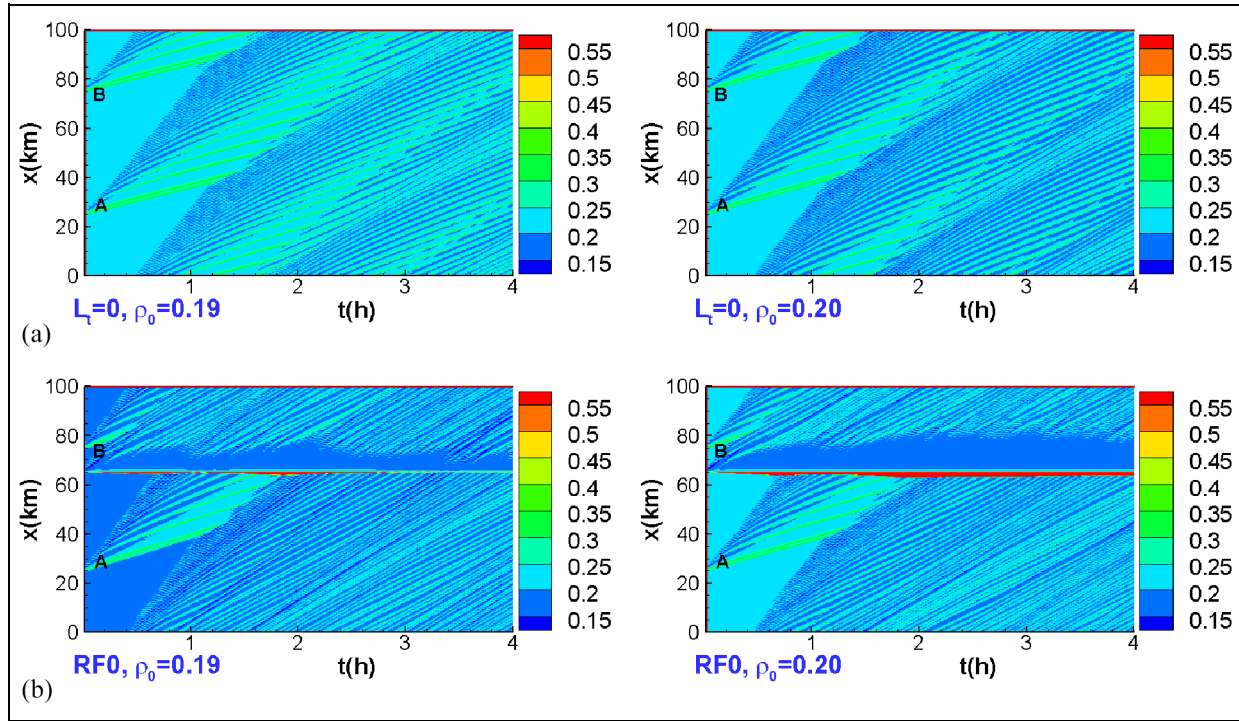
To determine whether there is a traffic shock triggered by the freeway tunnel, our approach is to determine the density threshold of traffic shock formation by examining the spatiotemporal evolution of traffic density on the freeway. From Figure 7(a), traffic flow patterns in the case without the freeway tunnel effects can be seen. While from Figure 7(b) for the case without ramp effects, one can ascertain

that the structure of vehicular flow patterns and relevant values of  $\rho_{th}$  are 0.20 in the units of jam density  $\rho_m$ .

Spatiotemporal evolutions of traffic density on the ring road in the case with ramp effects are shown in Figure 8(a) and (b), and it is seen that the values of  $\rho_{th}$  are 0.21 for RF2 and 0.23 for RF4, consistent with those given in Table 5. Increasing of the on ramp flow can also trigger a traffic shock propagating in the upstream direction.

**Table 5.** Density threshold of shock formation when the tunnel speed limit is 80 km/h.

Case	RF0	RF1	RF2	RF3	RF4
$\rho_{th}$	0.2	0.2	0.21	0.22	0.23

**Figure 7.** Spatiotemporal evolution of  $\rho_1$  in the case without ramp effects: (a)  $L_t = 0$ ,  $\rho_0 = 0.19, 0.20$  and (b) RF0,  $\rho_0 = 0.19, 0.20$ .

#### 4.6. Vehicle fuel consumption

To estimate vehicle fuel consumption, time-averaged grid speed of traffic flow is used, together with the car-performance diagram shown in Figure 9, which is assumed with respect to the performance diagram of Focus cars. Obviously, the fuel consumption is gear number dependent. When the car speed is over  $0.4 v_{f2}$ , i.e., 40 km/h, the gear number is set as 5. While when the car speed is ranged from 10 to 30 km/h, the gear number is 2, which has a number of 3 or 4 when the car speed is in the range from 30 to 40 km/h, depending on if the car speed is close to 40 km/h. For a lower car speed, such as below 10 km/h, the gear number is 1. Therefore, the car-performance curve has a general property of cars and based on a common recognition of cars in the real world.

With the mean grid speed by  $\bar{u}_{l,i}$ , making linear interpolation on the basis of the car-performance diagram gives the grid vehicle fuel consumption  $fc_{l,i}$ , the vehicle fuel

consumption of vehicles on lane  $l$  through the ring road is its sum

$$Fu_l = \sum_{i=1}^{l_{max}} fc_{l,i} \Delta x_i \quad (21)$$

as shown in Figure 10, the presence of tunnel affects  $Fu_l$  significantly when the initial density exceeds the density threshold of traffic shock formation. Otherwise, its influence is rather small, as can be seen in Table 6, where the data given in the second and third columns correspond to the thin blue and purple curves of Figure 10, and those data in the fourth and fifth columns are used to draw the coarse black and green curves of Figure 10, while the delta and circle symbols for the case of RF4 in Figure 10 are illustrated just for the effect of ramp flow. In particular, for  $\rho_0 = 0.5$ ,  $Fu_l$  has a lower value for the case without tunnel  $L_t = 0$ . Generally, for  $\rho_0 > \rho_{th}$ , the tunnel cause

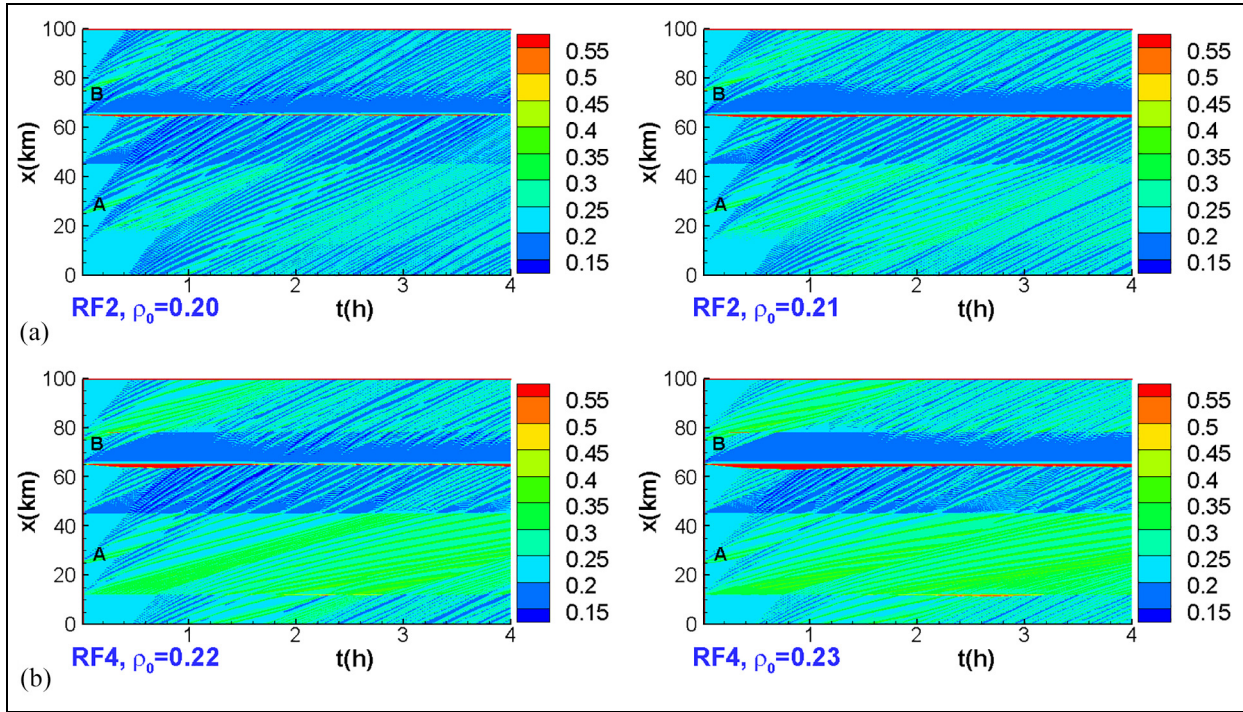


**Figure 8.** Spatiotemporal evolution of  $\rho_1$  in the case with ramp effects: (a) RF2,  $\rho_0 = 0.20, 0.21$  and (b) RF4,  $\rho_0 = 0.22, 0.23$ .

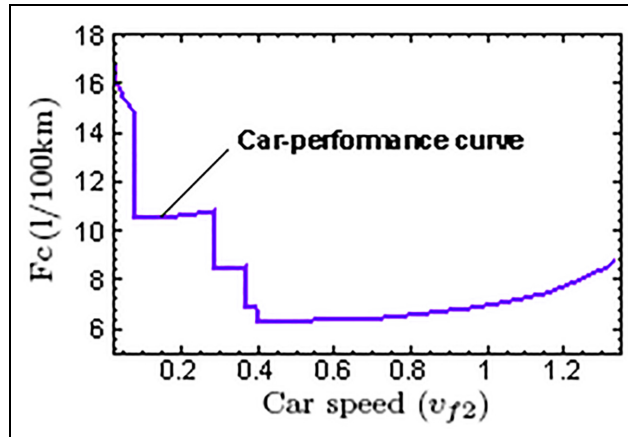


**Figure 9.** Car-performance diagram.

more fuel consumption in comparison with that for the case of  $L_t = 0$ , the amount of the more fuel consumption is  $\rho_0$ -dependent, as shown in Table 6.

## 5. Conclusion

To explore freeway tunnel effects on vehicular flow, a two-lane traffic model (TLM) is put forward. TLM equations are used to build a simulation platform, where a third-order Runge–Kutta scheme is used to handle the time

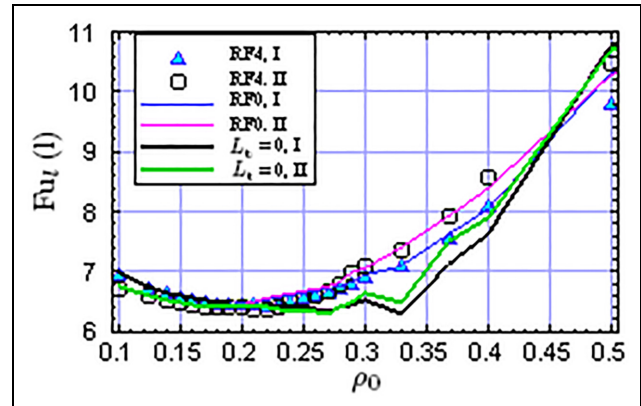


**Figure 10.**  $\rho_0$ -dependence of fuel consumption  $F_{u1}$  through the ring road.

derivative term and a fifth-order weighted essentially non-oscillatory scheme (WENO5) to calculate numerical flux. To validate TLM, two speed trajectories at the Kobotoko tunnel in Japan<sup>35</sup> as well as the simulated speed on the basis of a behavioral kinematic wave model<sup>36</sup> are used. From extensive numerical tests, the following conclusions are made:

1. TLM is capable of exploring freeway tunnel effects on traffic flow, and it can be applied to

**Table 6.** Distributions of  $F_{u_i}$  through the ring road without ramp effects. [AQ: 5]

$\rho_0$	RF0		$L_t = 0$	
	$F_{u_1}$ [l]	$F_{u_2}$	$F_{u_1}$	$F_{u_2}$
0.1	6.9695	6.7421	6.9726	6.7397
0.125	6.7467	6.6057	6.7479	6.6064
0.14	6.6508	6.5355	6.6523	6.5365
0.15	6.5979	6.4927	6.5982	6.4926
0.16	6.5524	6.4483	6.5527	6.4479
0.17	6.5143	6.4102	6.5110	6.4062
0.18	6.4836	6.4040	6.4697	6.3966
0.19	6.4509	6.4130	6.4295	6.3966
0.2	6.4666	6.4554	6.3972	6.3966
0.21	6.4867	6.5005	6.3966	6.3966
0.22	6.5162	6.5457	6.3966	6.3928
0.23	6.5482	6.5863	6.3966	6.3657
0.24	6.5831	6.6178	6.3966	6.3465
0.25	6.6203	6.6669	6.3913	6.3321
0.26	6.6594	6.7113	6.3664	6.3185
0.27	6.6961	6.7600	6.3479	6.3095
0.28	6.7395	6.8375	6.3926	6.3928
0.29	6.8335	6.9587	6.4516	6.4891
0.3	6.9236	7.0648	6.5334	6.6293
0.33	7.0821	7.3838	6.3120	6.4938
0.368	7.6154	7.927	7.1472	7.5137
0.4	8.0210	8.3956	7.6040	7.8975
0.5	10.3031	10.2925	10.7657	10.6911

The unit of fuel consumption  $F_{u_i}$  is liters (l).

2. TLM adopts a lane-changing time to describe the net lane-changing rate, while assuming that when the absolute value of density difference between the two lanes is lower than 1 veh/km, the lane changing time is infinite, otherwise, it is approximately equal to the traffic relaxation time. In comparison with existing modules of lane-changing, the present lane-changing module is possibly the simplest that can be adopted to explore freeway tunnel effects.
3. Under conditions of traffic flow simulation in this paper, when the freeway tunnel length is 0.3 km, if there is a tunnel triggered traffic shock, and the initial density normalized by jam density is less than 0.5, the mean tunnel travel time is approximately 0.0125 h, suggesting that the mean traffic flow speed in the tunnel is around 24 km/h.
4. There is a density threshold of shock formation, which can be determined by examining the spatio-temporal evolution of traffic density on the freeway, but depends on the off-ramp flow just upstream the tunnel.
5. When initial density is above the density threshold of shock formation, tunnel affects the vehicle fuel consumption significantly. Generally, vehicles need more fuel consumption to run through the ring road in comparison with the case without tunnel. But for larger normalized initial density such as 0.5, the situation is just the opposite.

### Acknowledgements

We thank Professor X.Y. Yin at USTC and Dr Y.-L. Li at Peking University for some useful private communications.

### Funding

The author(s) disclosed receipt of the following financial support for the research, authorship, and/or publication of this article: This work was supported by National Natural Science Foundation of China (Grant 11972341) and fundamental research project of Lomonosov Moscow State University “Mathematical models for multi-phase media and wave processes in natural, technical and social systems.”

### ORCID iD

Zuojin Zhu  <https://orcid.org/0000-0003-0777-8723>

## References

1. Hu ZJ, Smirnova MN, Zhang YL, et al. Estimation of travel time through a composite ring road by a viscoelastic traffic flow model. *Math Comput Simul* 2021; 181: 501–521.
2. Goñi-Ros B, Knoop VL, van Arem B, et al. Mainstream traffic flow control at sags. *Transp Res Rec: J Transp Res Board* 2014; 2470: 57–64.
3. Goñi-Ros B, Knoop VL, Takahashi T, et al. Optimization of traffic flow at freeway sags by controlling the acceleration of vehicles equipped with in-car systems. *Transp Res Part C: Emerg Technol* 2016; 71: 1–18.
4. Jin WL and Zhang HM. The formation and structure of vehicle clusters in the Payne-Whitham traffic flow model. *Transp Res Part B: Methodol* 2003; 37: 207–223.
5. Tympakianakia A, Koutsopoulos HN and Jenelius E. Anatomy of tunnel congestion: causes and implications for tunnel traffic management. *Tunnell Underground Space Technol* 2019; 83: 498–508.
6. Michalopoulos PG, Beskos DE and Yamauchi Y. Multilane traffic flow dynamics: some macroscopic considerations. *Transp Res Part B: Methodol* 1984; 18: 377–395.
7. Chang GL and Zhu ZJ. A macroscopic traffic model for highway work zones: formulations and numerical results. *J Advanced Transp* 2006; 40: 265–287.
8. Daganzo CF. A behavioral theory of multi-lane traffic flow: part i: long homogeneous freeway sections. *Transp Res Part B: Methodol* 2002; 36: 131–158.
9. Daganzo CF. A behavioral theory of multi-lane traffic flow: part ii: merges and on set of congestion. *Transp Res Part B: Methodol* 2002; 36: 159–169.
10. Tang TQ, Wong SC, Huang HJ, et al. Macroscopic modeling of lane-changing for two-lane traffic flow. *J of Advanced Transp* 2008; 43: 245–273.
11. Tang TQ, Wang YP, Yang XB, et al. A multilane traffic flow model accounting for lane width, lane-changing and the number of lanes. *Netw Spat Economic* 2014; 14: 465–483.
12. Smirnova MN, Bogdanova AI, Smirnov NN, et al. Multi-lane unsteady-state traffic flow models. *J Mechatronics* 2014; 2: 1–5.
13. Pour IM and Nassiri H. A macroscopic traffic flow model that includes driver sensitivity to the number of free spaces ahead. *Transportmetrica B: Transport Dynamics* 2020; 8: 290–306.
14. Pan TL, Lam WHK, Sumalee A, et al. Multiclass multilane model for freeway traffic mixed with connected automated vehicles and regular human-piloted vehicles. *Transportmetrica A: Transport Science* 2021; 17: 5–33.
15. Li L and Chen XQ. Vehicle headway modeling and its inferences in macroscopic/ microscopic traffic flow theory: a survey. *Transp Res Part C: Emerg Technol* 2017; 76: 170–188.
16. Liu H, Kan XG, Shladover SE, et al. Modeling impacts of cooperative adaptive cruise control on mixed traffic flow in multi-lane freeway facilities. *Transp Res Part C: Emerg Technol* 2018; 95: 261–279.
17. Jia D, Ngoduy D and Vu HL. A multiclass microscopic model for heterogeneous platoon with vehicle-to-vehicle communication. *Transportmetrica B: Transport Dynamics* 2019; 7: 311–335.
18. Zheng ZD. Recent developments and research needs in modeling lane changing. *Transp Res Part B: Methodol* 2014; 60: 16–32.
19. Laval JA and Daganzo CF. Lane-changing in traffic streams. *Transp Res Part B: Methodol* 2006; 40: 251–264.
20. Jin WL. Akinematic wave theory of lane-changing traffic flow. *Transp Res Part B: Methodol* 2010; 44: 1001–1021.
21. Jin WL. A multi-commodity Lighthill-Whitham-Richards model of lane-changing traffic flow. *Transp Res Part B: Methodol* 2013; 57: 361–377.
22. Zheng Z, Ahn S, Chen D, et al. Freeway traffic oscillations: microscopic analysis of formations and propagations using Wavelet Transform. *Transp Res Part B: Methodol* 2011; 45: 1378–1388.
23. Cassidy M and Rudjanakanoknad J. Increasing the capacity of an isolated merge by metering its on-ramp. *Transp Res Part B: Methodol* 2005; 39: 896–913.
24. Delis AI, Nikolos IK and Papageorgiou M. High-resolution numerical relaxation approximations to second-order macroscopic traffic flow models. *Transp Res Part C: Emerg Technol* 2014; 44: 318–349.
25. Jin S and Xin ZP. The relaxation schemes for systems of conservation laws in arbitrary space dimensions. *Commun Pure Appl Math* 1995; XLVIII: 235–276.
26. Borges R, Carmona M, Costa B, et al. An improved weighted essentially non-oscillatory scheme for hyperbolic conservation laws. *J Comput Phys* 2008; 227: 3191–3211.
27. Rao RS, Park SY and Chang GL. Developing the guidelines for managing autonomous vehicle flows on congested highways: a case study of md-100. *Simulation* 2021; 97: 367–382.
28. Singh MK and Rao KR. Selection of open or closed boundaries in a cellular automata model for heterogeneous non-lane-based traffic. *Simulation*. Epub ahead of print 22 February 2022. DOI: 10.1177/00375497221078936.
29. Zhang Y, Tian HW, Li R, et al. Hybrid simulation model for navigation performance evaluation of the three Gorges-Gezhouba Dams under novel regulations. *Simulation* 2022; 98: 677–698.
30. Kiselev AB, Nikitin NF, Smirnov NN, et al. Irregular traffic flow on a ring road. *J Appl Math Mech* 2000; 64: 627–634.
31. Shu CW. Total-variation-diminishing time discretizations. *SIAM J Sci Statis Comput* 1988; 9: 1073–1084.
32. Shu CW and Osher S. Efficient implementation of essentially non-oscillatory shock-capturing schemes. *J Comput Phys* 1989; 83: 32–78.
33. Jiang GS and Shu CW. Efficient implementation of weighted eno schemes. *J Comput Phys* 1996; 126: 202–228.
34. Henrick AK, Aslam TD and Powers JM. Mapped weighted essentially non-oscillatory schemes: achieving optimal order near critical points. *J Comput Phys* 2005; 207: 542–567.
35. Koshi M, Kuwahara M and Akahane H. Capacity of sags and tunnels on Japanese motorways. *ITE J* 1992; 62: 17–22.
36. Jin WL. Kinematic wave models of sag and tunnel bottlenecks. *Transp Res Part B: Methodol* 2018; 107: 41–56.
37. Zhang YL, Smirnova MN, Bogdanova AI, et al. Travel time estimation by urgent-gentle class traffic flow model. *Transp Res Part B: Methodol* 2018; 113: 121–142.
38. Zhu ZJ and Yang C. Visco-elastic traffic flow model. *J Advanced Transp* 2013; 47: 635–649.

39. Bogdanova A, Smirnova MN, Zhu ZJ, et al. Exploring peculiarities of traffic flows with a viscoelastic model. *Transportmetrica A: Transport Science* 2015; 11: 561–578.
40. Ma J, Chan CK, Ye ZB, et al. Effects of maximum relaxation in viscoelastic traffic flow modeling. *Transp Res Part B: Methodol* 2018; 113: 143–163.
41. Zhang YL, Smirnova MN, Bogdanova AI, et al. Travel time prediction with a viscoelastic traffic model. *Applied Math & Mech (English Edition)* 2018; 39: 1769–1788.
42. Zhu ZJ and Wu TQ. Two-phase fluids model for freeway traffic and its application to simulate the evolution of solitons in traffic. *ASCE J Transp Engineering* 2003; 129: 51–56.
43. Zhang YL, Smirnova MN, Ma J, et al. Freeway tunnel effect of travel time based-on a double lane traffic model. *Int J Transp Sci Technol* 2022; 11: 360–380.
44. Shui HS. TVD scheme. In: Shui HS (ed.) *Finite difference in one-dimensional fluid mechanics*. Beijing, China: National Defense, 1998, pp. 333–355 (in Chinese).
45. Smirnova MN, Bogdanova AI, Zhu ZJ, et al. Traffic flow sensitivity to visco-elasticity. *Theoret Appl Mech Lett* 2016; 6: 182–185.
46. Smirnova MN, Bogdanova AI, Zhu ZJ, et al. Traffic flow sensitivity to parameters in viscoelastic modelling. *Transportmetrica B: Transport Dynamics* 2017; 5: 115–131.
47. Zhang YL, Smirnova MN, Ma J, et al. Tunnel effects on ring road traffic flow based on an urgent-gentle class traffic model. *Theoret Appl Mech Lett* 2021; 11: 100283.
48. Chang GL and Mahmassani HS. Travel time prediction and departure time adjustment behavior dynamics in a congested traffic system. *Transp Res Part B: Methodol* 1988; 22: 217–232.
49. Wang DH, Fu FJ, Luo XQ, et al. Travel time estimation method for urban road based on traffic stream directions. *Transportmetrica A: Transport Science* 2016; 12: 497–503.

### Author biographies

**Zhengming Li** has been an associate professor in the School of Information Science and Technology of USTC

since 2002. He has taken part in the project NSFC 11962311 and carried out some studies on traffic flow modeling.

**M N Smirnova** is an associate professor in Faculty of Mechanics and Mathematics of Lomonosov Moscow State University (LMSU). She received her PhD degree in Physics and Mathematics from LMSU in the year 2013. Currently, she has done some studies in fluid mechanics and transportation engineering. Now she has the interest in mathematical modeling multi-phase media and wave processes in natural, technical, and social systems

**Yongliang Zhang** is an associate professor in Faculty of Engineering Science of USTC. He obtained his PhD degree in 2018 at USTC and worked as a postdoctoral researcher at USTC during 2018–2020. His current research interest is mainly in engineering mechanics.

**N N Smirnov** is a professor in Faculty of Mechanics and Mathematics of Lomonosov Moscow State University (LMSU). He received his MS and PhD degrees in Physics and Mathematics from LMSU in the years 1976 and 1980, respectively, Habilitated Doctor degree in 1990, and has been an academician of Russian Academy of Natural Sciences since 2007.

**Zuojin Zhu** is an associate professor in Faculty of Engineering Science of USTC. He obtained his PhD degree in 1990 at Shanghai Jiao Tong University and worked as a research fellow at the Hong Kong Polytechnic University in 2008. His current research interest is mainly in thermal fluid flow and transportation engineering fields.